



Identification and Structural Characterization of the Precursor Conformation of the Prion Protein which Directly Initiates Misfolding and Oligomerization

Roumita Moulick and Jayant B. Udgaonkar

National Centre for Biological Sciences, Tata Institute of Fundamental Research, Bengaluru 560065, India

Correspondence to Jayant B. Udgaonkar: jayant@ncbs.res.in

<http://dx.doi.org/10.1016/j.jmb.2017.01.019>

Edited by Ronald Wetzel

Abstract

To identify and structurally characterize the precursor conformation of the prion protein (PrP), from which misfolding and aggregation directly commence, has been a long-standing goal. Misfolding converts the α -helical, non-pathogenic functional form of PrP to pathogenic, β -structured oligomeric and amyloidogenic forms, which are the cause of prion diseases. Susceptibility to sporadic prion disease correlates well with the propensity of PrP to misfold to cytotoxic, proteinase K resistant oligomeric conformations at low pH. In this study, mutagenesis at the hydrophobic core of the mouse PrP has been shown to stabilize a monomeric unfolding intermediate (I), which is populated significantly at equilibrium at low pH. Importantly, the rate of formation of β -structured oligomers at low pH is found to correlate well with the extent to which this intermediate is populated. The misfolding process is limited by the dimerization of I, indicating that I is the monomeric precursor conformation that directly initiates misfolding. Structural and thermodynamic characterization by native-state hydrogen–deuterium exchange mass spectrometry studies indicate that the precursor conformation is a partially unfolded form of PrP that forms under misfolding-prone solvent conditions.

© 2017 Elsevier Ltd. All rights reserved.

Introduction

The misfolding of the cellular prion protein (PrP; PrP^C) into toxic oligomers or fibrillar forms collectively termed scrapie PrP (PrP^{Sc}) is the primary cause of transmissible spongiform encephalopathies (TSE) which are a group of fatal neurodegenerative diseases [1]. *In vivo*, prionopathies may occur due to genetic mutations of the Prnp gene, which enhance the aggregation propensity of the protein, or through infection by diseased PrP^{Sc} forms, which then act as a template for the autocatalytic conversion of PrP^C into PrP^{Sc}. However, most reported spongiform encephalopathies are the result of spontaneous conversion of PrP^C into PrP^{Sc} [2]. Although the mechanism of this spontaneous conformational conversion is not understood, various studies *in vitro* have indicated that the conformational flexibility of the native (N) state of the PrP is a crucial factor in initiating aggregation [3–6].

High conformational flexibility facilitates fluctuations to partially unfolded, high energy intermediates, which may have solvent-exposed hydrophobic residues that can act as nucleation sites for aggregation

[7,8]. Indeed, for the PrP, partially structured or molten globule-like conformations have been implicated as potential precursors of oligomerization [3,9–13]. It has also been suggested that aggregation initiates from a β -rich monomer that is a conformational isoform of the α -helical monomer [14–16]. Since aggregation is initiated by spontaneous conformational conversion of the native protein, it is crucial to understand the energetics and structure of the key molecular species in the native conformational ensemble, from which misfolding and aggregation commence.

The native conformational ensemble is dominated by the structural characteristics of the native state, and determining the properties of high energy, partially unfolded forms of the protein is difficult, as they are not populated to any significant extent. Nevertheless, such transiently populated intermediates have been shown to play a crucial role in initiating aggregation for several proteins [7]. Relaxation dispersion NMR measurements [17], thiol-labeling studies [18,19], and, in particular, native-state hydrogen-deuterium exchange (HDX) studies [20–22] have provided direct structural insights into high energy states of proteins.

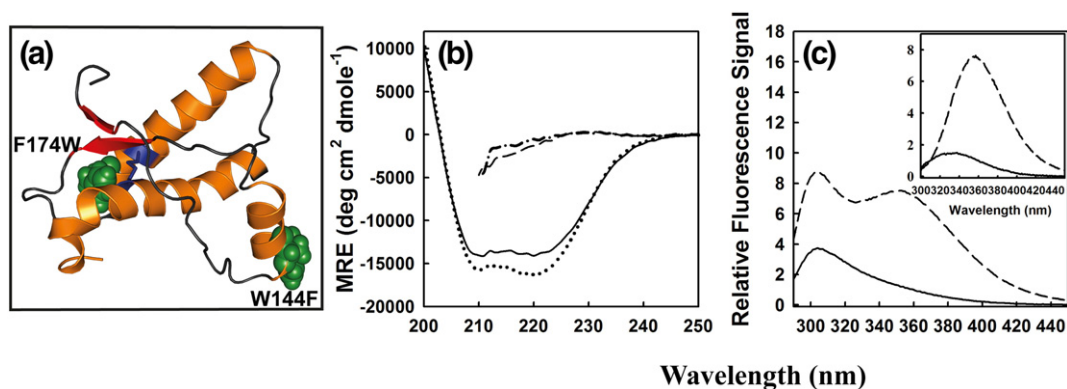


Fig. 1. Structural and spectroscopic characterization of dm CTD. Panel (a) shows residues W144 and F174 in the C-terminal domain of moPrP (121-231) in green, which were mutated to obtain W144F/F174W moPrP (121-231) referred to as dm CTD. The α -helices are shown in orange, β -strands in red, and loops in gray. Residues C178 and C213, linked by the disulfide bond, are shown in blue. Panel (b) shows the CD spectra of native (dotted line) and unfolded (dot/dash line) dm CTD, along with the CD spectra of native (solid line) and unfolded (dashed line) dm CTD at pH 4 and at 25 °C. Panel (c) shows the relative fluorescence spectra of native (solid line) and unfolded (dashed line) dm CTD upon excitation at 280 nm at pH 4 and 25 °C. The inset shows the fluorescence spectra of native (solid line) and unfolded (dashed line) dm CTD upon excitation at 295 nm at pH 4 and 25 °C. The fluorescence spectra have been normalized to the fluorescence signal of native protein at 360 nm.

In the case of mouse PrP (moPrP), a native-state HDX study under solvent conditions that promote misfolding to β -rich oligomers showed that the N state existed in equilibrium with at least two partially unfolded forms (PUFs), PUF1 and PUF2, which were populated to extremely minor extents [6]. These PUFs were not observed under experimental conditions where the propensity to aggregate was much lower or negligible [23,24]. Of the two PUFs, the identity of the PUF initiating aggregation has, however, remained ambiguous.

To determine whether either of these PUFs, or another high energy intermediate, might be the key monomeric species from which spontaneous conversion of PrP^C into PrP^{Sc} begins, it is necessary to first stabilize the intermediate so that it becomes populated to a significant extent at equilibrium. High energy conformations of proteins can be stabilized either by changing solvent conditions [25,26] or by mutation [27,28]. A mutational approach would be useful in the case of the PrP, as the kinetics of misfolding could then be correlated to the extent to which the high energy conformation is populated, under solvent conditions that promote misfolding.

In this study, a double mutant variant [W144F/F174W moPrP (121-231) or double mutant variant of the C-terminal domain (CTD; dm CTD)] of the CTD of moPrP (Fig. 1a) was found, fortuitously, to populate a monomeric equilibrium unfolding intermediate, I, at pH 4 where the protein is prone to misfolding to β -rich oligomers [29]. Such oligomers formed at low pH have been shown to disrupt lipid membranes [29], and the propensity for sporadic prion disease has been found to correlate well with the extent to which they are populated [16]. I could not be detected at

pH 7 where the protein is not prone to misfolding, in agreement with earlier studies [30,31]. Three-state analysis of the equilibrium unfolding transition of dm CTD suggested that both the structural characteristics and stability of I with respect to N were similar to those of PUF2, which was found by native-state HDX studies carried out at different urea concentrations to be populated in equilibrium with the N state. Thus, the intermediate I, stabilized by mutation in dm CTD, could be identified as PUF2. Most importantly, the rate of misfolding was found to correlate positively with the fractional population of PUF2/I, suggesting that misfolding commences directly from this PUF of dm CTD.

Results

dm CTD was observed to retain the secondary structure of wild-type (wt) CTD (Fig. 1b) but exhibited a \sim 7-fold increase in fluorescence at 360 nm upon unfolding (Fig. 1c), as had been observed previously [30]. It seems that the fluorescence of W174 is quenched by the native disulfide bond between C178 and C213 in the N state of dm CTD [32] and that this quenching is relieved upon unfolding.

The urea-induced unfolding transition of dm CTD, monitored by a change in CD at 222 nm and by a change in fluorescence upon unfolding, was found to be reversible at 25 °C, at both pH 4 and pH 7. At pH 4, the two probes yielded unfolding transitions that were non-coincident (Fig. 2a). Secondary structure was lost at lower urea concentrations and tertiary structure at higher urea concentrations. Such non-coincident unfolding transitions indicated

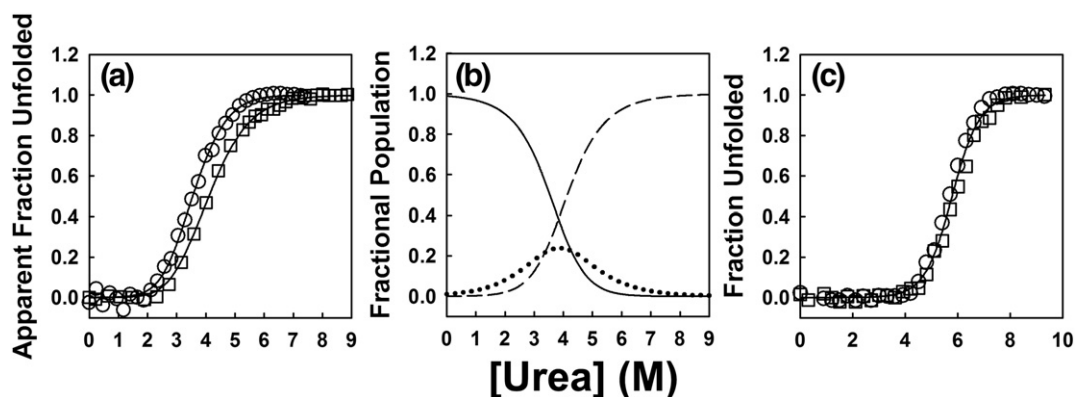


Fig. 2. Isothermal urea-induced unfolding of dm CTD. Panel (a) shows the isothermal urea-induced unfolding curves of dm CTD at 25 °C and pH 4, monitored by a change in mean residual ellipticity at 222 nm (circles) and by a change in tryptophan fluorescence at 360 nm upon excitation at 280 nm (squares). The solid lines through the data are non-linear least-squares fit to a three-state model given by Eq. (1). Panel (b) shows the dependences of the fractional populations of the native state (solid line), intermediate state (dotted line), and unfolded state (dashed line) on urea concentration. Panel (c) shows the urea-induced unfolding curves at 25 °C and at pH 7, monitored both by the measurement of mean residual ellipticity at 222 nm (circles) and by a measurement of fluorescence (squares) at 360 nm upon excitation at 280 nm.

that at least one equilibrium intermediate, I, is populated during unfolding [33].

The unfolding transition curves monitored by CD at 222 nm and by fluorescence were fit globally to a three-state $N \leftrightarrow I \leftrightarrow U$ unfolding model using Eqs. (1) and (3a) (3b). The global fit yielded values for ΔG_{IN}^0 of 2.7 ± 0.1 kcal mol⁻¹, ΔG_{UI}^0 of 1.9 ± 0.2 kcal mol⁻¹, and for m_{IN} and m_{UI} of 0.6 ± 0.03 kcal mol⁻¹ M⁻¹ and 0.59 ± 0.05 kcal mol⁻¹ M⁻¹, respectively, for dm CTD. The values for ΔG_{UN}^0 ($\Delta G_{IN}^0 + \Delta G_{UI}^0$) and m_{UN} ($m_{IN} + m_{UI}$) were not significantly different from the values for ΔG_{UN}^0 of 4.8 kcal mol⁻¹, and m_{UN} of 1.4 kcal mol⁻¹ M⁻¹, for wt CTD at pH 4 [5]. The fractional secondary structure content and fluores-

cence property of I were found to be $20 \pm 3\%$ and $90 \pm 10\%$, respectively, of that of the N state (Eq. (2)). This indicated that I had unfolded-like secondary structure and a native-like environment around W174. The parameters obtained from the fit were used to calculate the changes in the fractional populations of the N, I, and U states, with a change in urea concentration, using Eq. (4a), (4b), (4c) (Fig. 2b). I was found to be maximally populated to ~23% in 4 M urea.

In contrast, the CD and fluorescence-monitored urea-induced equilibrium unfolding transitions were completely coincident at pH 7 (Fig. 2c), indicating that I was not populated sufficiently to be detected

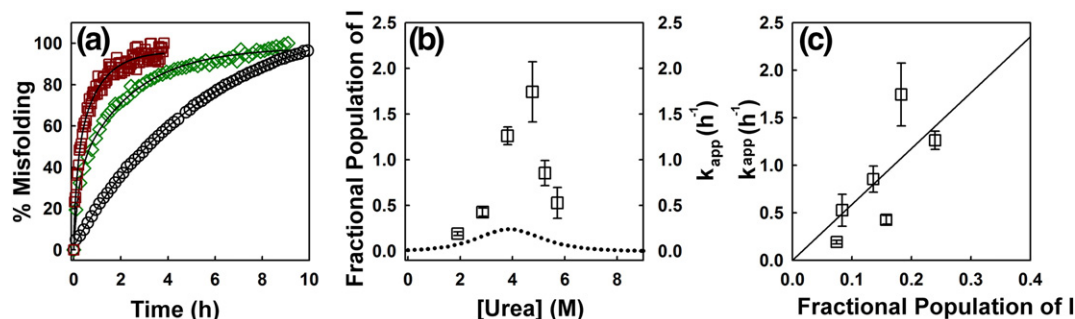


Fig. 3. Kinetics of misfolding of dm CTD initiated by the addition of NaCl at pH 4. Panel (a) shows representative kinetic traces of misfolding of 50 μ m dm CTD at pH 4 and at 25 °C in the presence of 2 M (black circles), 5 M (dark red squares), and 6 M (green diamonds) urea and 150 mM NaCl. Misfolding was monitored by the measurement of the CD signal at 215 nm. The solid lines are exponential fits through the data. Panel (b) shows the dependence of the apparent rate of misfolding (squares) on urea concentration. The dotted line shows the fractional population of the intermediate. Panel (c) shows the dependence of the apparent rate of misfolding (squares) on the fractional population of the intermediate. The solid line is a linear least-squares fit through the data. In all cases, the error bars represent the mean \pm SD obtained from three independent experiments.

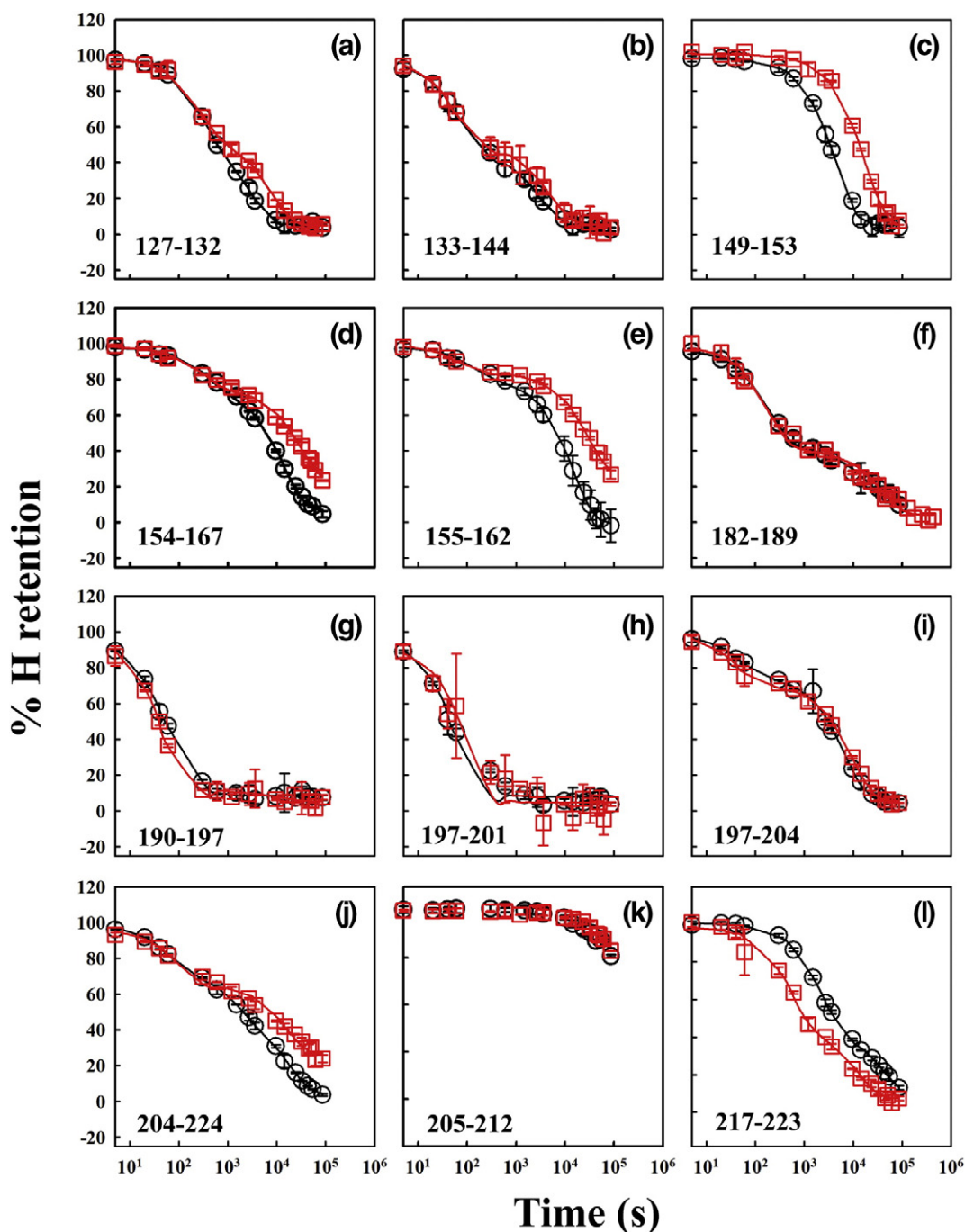


Fig. 4. HDX-MS of wt CTD and dm CTD in D₂O at 25 °C and at pD 4. Panels (a–l) show the % hydrogen retention *versus* time data for the 12 peptide fragments: 127-132, 133-144, 149-153, 154-167, 155-162, 182-189, 190-197, 197-201, 197-204, 204-224, 205-212, and 217-223 of wt CTD (red squares) and dm CTD (black circles) in the absence of any denaturant. The solid lines in red and black are the exponential decay fits through the wt CTD and dm CTD data, respectively. The error bars represent the mean \pm SD obtained from two independent experiments.

at pH 7. The two-state transition observed at pH 7 for dm CTD yielded values for ΔG^0_{UN} and m_{UN} of 6.9 kcal mol⁻¹ and 1.1 kcal mol⁻¹ M⁻¹, respectively, which were similar to the values for ΔG^0_{UN} and m_{UN} of 7.3 kcal mol⁻¹ and 1.2 kcal mol⁻¹ M⁻¹ for wt CTD at pH 7 [5].

To investigate if I was monomeric or oligomeric, urea-induced equilibrium unfolding transitions were monitored at different protein concentrations ranging from 5 to 50 μ M, by CD at 222 nm and by fluorescence. In all cases, the observed equilibrium unfolding transitions overlapped completely with each other

Table 1. Parameters obtained from native-state HDX into wt CTD and dm CTD at pD 4 and at 25 °C

Secondary Structure	Sequence Segment	k_{int} (s^{-1})	k_{obs} (s^{-1}) wt CTD	k_{obs} (s^{-1}) dm CTD	ΔG_{op}^0 wt CTD	ΔG_{op}^0 dm CTD	$\Delta\Delta G_{\text{op}}^0$ wt-dm CTD
$\beta 1$	127-132	4×10^{-3}	$(1.3 \pm 0.1) \times 10^{-4}$	$(3.4 \pm 0.2) \times 10^{-4}$	$2.0 \pm 0.05(0.4)^*$	$1.5 \pm 0.03(0.3)^*$	0.5
Loop between $\beta 1$ and $\alpha 1$	133-143	9×10^{-4}	$(1.9 \pm 0.02) \times 10^{-4}$	$(3.1 \pm 0.6) \times 10^{-4}$	$0.9 \pm 0.01(0.3)^*$	$0.7 \pm 0.1(0.3)^*$	0.2
$\alpha 1$	133-148	5.8×10^{-3}	$(1.1 \pm 0.1) \times 10^{-4}$	–	$2.3 \pm 0.07(0.4)^*$	–	–
	144-148	8.3×10^{-3}	–	$(1.3 \pm 0.01) \times 10^{-4}$	–	$2.5 \pm 0.01(0.6)^{\#}$	–
	149-153	0.01	$(5.6 \pm 0.2) \times 10^{-5}$	$(2.2 \pm 0.02) \times 10^{-4}$	$3.1 \pm 0.02(0.7)^{\#}$	$2.4 \pm 0.01(0.7)^{\#}$	0.7
Loop between $\alpha 1$ and $\alpha 2$, including $\beta 2$ strand	154-167	3.9×10^{-3}	$(3.1 \pm 0.2) \times 10^{-5}$	$(7.3 \pm 0.3) \times 10^{-5}$	$2.9 \pm 0.04(0.7)^{\#}$	$2.3 \pm 0.03(0.6)^{\#}$	0.6
	155-162	3.8×10^{-3}	$(3.2 \pm 0.4) \times 10^{-5}$	$(6.7 \pm 0.1) \times 10^{-5}$	$2.8 \pm 0.08(0.7)^{\#}$	$2.4 \pm 0.01(0.5)^{\#}$	0.4
$\alpha 2$	182-189	5.5×10^{-3}	$(5 \pm 3) \times 10^{-5}$	$(7.4 \pm 2.8) \times 10^{-4}$	$2.6 \pm 0.2(0.8)^{\#}$	$2.6 \pm 0.2(0.3)^*$	0
Loop between $\alpha 2$ and $\alpha 3$	190-197	8.4×10^{-3}	$(8.8 \pm 7.2) \times 10^{-3}$	$(8.8 \pm 5.2) \times 10^{-3}$	–	–	–
	197-201	9.4×10^{-3}	$(2 \pm 0.2) \times 10^{-2}$	$(1.6 \pm 0.2) \times 10^{-2}$	–	–	–
$\alpha 3$	197-204	3.1×10^{-3}	$(1.0 \pm 0.04) \times 10^{-4}$	$(1.5 \pm 0.1) \times 10^{-4}$	$2.0 \pm 0.02(0.3)^*$	$1.8 \pm 0.05(0.4)^*$	0.2
	204-224	8.1×10^{-3}	$(4.2 \pm 0.2) \times 10^{-4}$	$(6.4 \pm 0.02) \times 10^{-4}$	$1.7 \pm 0.3(1)^{\#}$	$1.6 \pm 0.01(0.1)^*$	0.1
			$(2.8 \pm 0.9) \times 10^{-5}$	$(5.4 \pm 0.6) \times 10^{-5}$	$3.4 \pm 0.2(0.9)^{\#}$	$3 \pm 0.06(0.6)^{\#}$	0.4
	205-212	6.8×10^{-3}	$(2.1 \pm 0.1) \times 10^{-6}$	$(2.1 \pm 0.1) \times 10^{-6}$	$4.9 \pm 0.05(1.1)^{\#}$	$4.9 \pm 0.05(1.1)^{\#}$	0
217-223	5.3×10^{-3}	$(1.1 \pm 0.2) \times 10^{-4}$	$(4.4 \pm 0.2) \times 10^{-4}$	–	$1.6 \pm 0.04(0.1)^*$	–	
				$(2.3 \pm 0.04) \times 10^{-5}$	$2.3 \pm 0.1(0.3)^*$	$3.4 \pm 0.01(0.6)^{\#}$	–0.9

The stabilities of the peptic fragments corresponding to sequence segments of wt and dm CTD were calculated from the rates of exchange obtained from native-state HDX-MS. The rates of the slow kinetic phases of exchange for the sequence segments of wt CTD and dm CTD, obtained from native-state HDX-MS, are reported here as mean \pm SD from two independent experiments. The ΔG_{op}^0 (in kcal mol $^{-1}$) and the m_{op} values (in kcal mol $^{-1}$ M $^{-1}$, reported in brackets) for each sequence segment were evaluated as described before [6]. Since the peptide corresponding to sequence segment 133-148 was not observed in dm CTD, HDX rate of the peptide corresponding to sequence segment 144-148 is reported. The slow-exchanging residues in each sequence segment were identified earlier [6]. The sequence segments, which exchange out in PUF1 and PUF2 in wt CTD and in dm CTD, are marked by “*” and “#”, respectively. For sequence segments 190–197 and 197–201, the dashes (–) indicate that none of the residues were observed to exchange slowly in the HDX-MS experiments.

(Fig. S1). The lack of dependence on protein concentration indicated that I was monomeric. To confirm the absence of any oligomers, which, for PrP, are known to induce a large increase in the fluorescence of 1-anilino-8-naphthalene sulfonate (ANS) upon binding to it [34], dm CTD was incubated with ANS in the presence of different concentrations of urea ranging from 0 to 8 M, as described in Materials and Methods. Figure S2a shows that in none of the experimental conditions was an increase in fluorescence intensity, or a blue shift of the emission maximum of ANS, observed, confirming that I was not oligomeric. Both size-exclusion chromatography measurements (Fig. S2b) and dynamic light scattering (DLS) measurements (data not shown) also indicated that no oligomers were present in 0, 4, and 6 M urea. Native dm CTD eluted out at \sim 12 mL, while the protein in 4 M and 6 M urea, which comprises both U and I (Fig. 2b) in fast exchange, eluted out as a single peak at \sim 10.6 mL and \sim 10 mL, respectively. The mean hydrodynamic radius (R_h) of dm CTD was 1.5 nm for the N state in the absence of urea, and 3.5 nm and 3.9 nm for protein in the presence of 4 M and 6 M urea, respectively.

In order to investigate the misfolding propensity of the N, I, and U states of dm CTD, the misfolding of 50 μ M dm CTD incubated in different concentrations of urea was initiated by the addition of NaCl,

as described previously [29] (see Materials and Methods). Figure 3a shows representative kinetic traces of % Misfolding of dm CTD, calculated using Eq. (5), in the presence of 2, 5, and 6 M urea and 150 mM NaCl. Apart from the kinetic trace of misfolding in 2 M urea, which fit well to a single exponential equation [Eq. (6a)], all the kinetic traces for misfolding fit best to a bi-exponential equation [Eq. (6b)] from which the apparent rate of misfolding could be calculated using Eq. (6c). At present, the origin of the observed bi-exponential kinetics is not known. Figure 3b shows the change in the apparent rate of misfolding with a change in urea concentration. The rate of misfolding was maximum at the urea concentration (4 M) at which I was maximally populated. Figure 3c shows that the apparent rate of misfolding increases linearly with an increase in the fractional population of I. The dependence of the initial rate of misfolding on the concentration of I formed at different urea concentrations by dm CTD was used to determine the reaction order of the misfolding reaction (see Materials and Methods). The order was estimated to be 2.45 (Fig. S3) with respect to I.

Under the experimental conditions (150 mM NaCl at 25 °C and at pH 4, in the presence of varying urea concentrations) used to misfold moPrP in this study, misfolding is known to be accompanied by

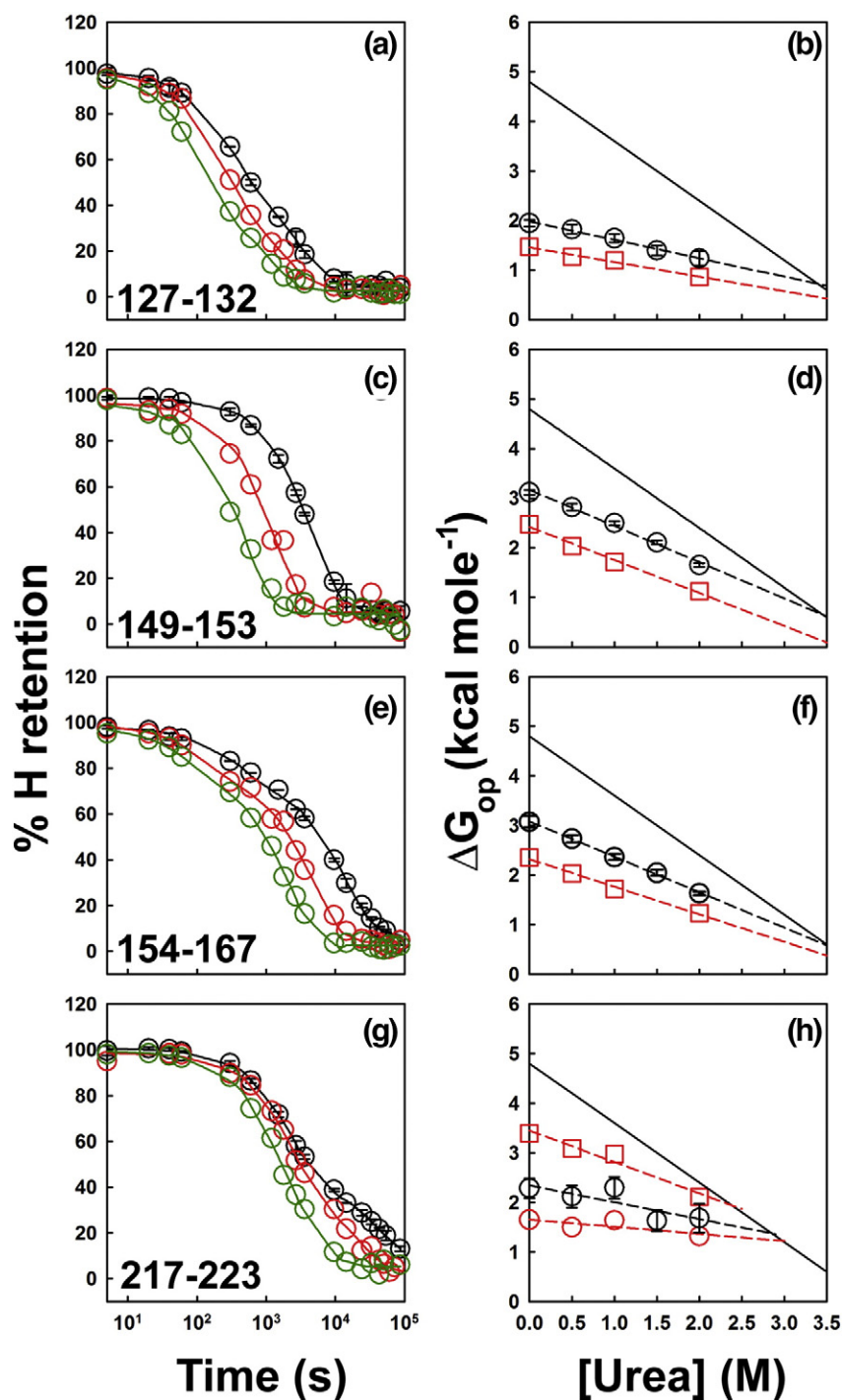


Fig. 5. HDX-MS of backbone amide hydrogens of dm CTD at pD 4 and 25 °C in the presence of 0 to 2 M urea. (a, c, e, and g) The % hydrogen retention *versus* time data for peptide fragments 127-132, 149-153, 154-167, and 217-223 in the presence of 0 (black circles), 1 (red circles), and 2 M (green circles) urea are shown. The solid lines in black, green, and red are the exponential decay fits to the 0, 1, and 2 M urea data, respectively. Panels (b, d, f, and h) show the denaturant dependences of ΔG_{op} of the peptide fragments 127-132, 149-153, 154-167, and 217-223 of dm CTD (squares and circles in red). The denaturant dependences of ΔG_{op} of these peptide fragments in the CTD of wt moPrP (23–231; black circles) are shown for comparison. The dashed lines in red and black are linear least-squares fits through the data for dm CTD and wt CTD, respectively, and the slopes yield the m_{op} values for the different segments. The solid line represents the dependence of global stability (ΔG_U) on the concentration of urea, with its slope given by m_U [5].

oligomerization [29]. Figure S4 shows the CD spectra of the oligomers formed at 3, 4, 5, and 5.5 M urea in the presence of 150 mM NaCl, collected after the misfolding and oligomerization reactions had reached saturation. The near-overlap of the CD spectra of these oligomers indicated not only that they were structurally similar, but importantly, that about the same extent of oligomerization had occurred at all urea concentrations. Moreover, in all cases, the R_h of these oligomers, as determined by DLS, was 7 nm (data not shown).

To structurally characterize I, which is populated to <1 % in native conditions (zero denaturant), a native-state HDX study of dm CTD was carried out. An earlier such study of wt CTD had shown that the N state existed in equilibrium with at least two PUFs, PUF1 and PUF2, which were populated to extremely minor extents [6]. These PUFs were not observed under experimental conditions where the propensity to aggregate was much lower or negligible [23,24]. Nevertheless, it could not be determined whether any one of these two PUFs was directly involved in initiating misfolding. The discovery that I directly initiates misfolding made it imperative to determine whether I was identical to either of these PUFs.

Native-state HDX mass spectrometry (HDX-MS) was therefore carried out on dm CTD in the presence of different concentrations of urea (0–2 M), as described before [6]. Significant differences in the exchange kinetics of peptides corresponding to sequence segments 127-132, 149-153, 154-167, 155-162, 204-224, and 217-223 were observed between dm CTD and wt CTD (Fig. 4). These sequence segments represent the $\beta 1$ region, the C-terminal region of $\alpha 1$, the $\alpha 1$ - $\beta 2$ - $\alpha 2$ loop, the $\beta 2$ region, the $\alpha 3$ region, and the C-terminal region of $\alpha 3$, respectively. Faster HDX kinetics for dm CTD, relative to wt CTD, were observed in the $\beta 1$ region, the C-terminal region of $\alpha 1$, the region between $\alpha 1$ and $\alpha 2$ including $\beta 2$, and in the central region of $\alpha 3$. This corresponds to a decrease in the free energy of structure opening to the exchange of sequence segments 127-132 and 149-153 by 0.5 kcal mol⁻¹ and 0.7 kcal mol⁻¹, respectively, and of sequence segments 155-162 and 154-167 by 0.4 kcal mol⁻¹ and 0.6 kcal mol⁻¹, respectively. The sequence segments 197-204 and 205-212, which correspond to the N-terminal and central regions of $\alpha 3$, were similarly stable in both the proteins (Fig. 4 and Table 1). However, segment 204-224 showed significant differences in stability between the two variants (Table 1). This indicated that the region 214-218, which forms the disulfide-bonded core of the protein and contains the slow-exchanging residues C213, T215, Q216, and Q218 [6] had lower protection factors in dm CTD than in wt CTD and was more dynamic and more solvent accessible in dm CTD. In contrast, the C-terminal region of $\alpha 3$ in dm CTD

showed slower exchange kinetics. The backbone amide hydrogens in this sequence segment of dm CTD exchanged out in two slow phases (Table 1). This region was less dynamic and consequently less accessible to solvent.

For each of the different structural regions of the two PrP variants (representative segments shown in Fig. 5), the change in accessible surface area accompanying exchange (listed in Table 1), measured by the m_{op} value, was obtained from a linear fit to the urea concentration dependence of the exchange kinetics and hence stability (ΔG_{op}). The m_{op} values indicated that two PUFs, PUF1 and PUF2, were populated by dm CTD in native conditions (Table 1), as shown for wt CTD in a previous study [6]. For dm CTD, PUF1 corresponds to sequence segments having an m_{op} value of 0.26 ± 0.09 kcal mol⁻¹ M⁻¹ and PUF2 corresponds to those sequence segments having an m_{op} value of 0.6 ± 0.05 kcal mol⁻¹ M⁻¹. Upon averaging the ΔG_{op}^0 values of the sequence segments exchanging in PUF1 and PUF2, their relative stabilities with respect to the N state, as deduced from the averaged ΔG_{op}^0 values, were determined to be 1.6 ± 0.6 kcal mol⁻¹ and 2.7 ± 0.4 kcal mol⁻¹, respectively. PUF1, with the lower ΔG_{op}^0 value, indicating that it is closer to N in energy, undergoes HDX faster than PUF2, with the higher ΔG_{op}^0 value.

The residues exchanging in PUF1 and PUF2 of dm CTD were identical to those exchanging in PUF1 and PUF2 of wt CTD, with the exception of residues in sequence segments 182-189, 204-224, and 217-223 (Table 1). Other than the residues in $\beta 1$, which exchanged out in PUF1, all the regions that showed lower ΔG_{op}^0 values exchanged out in PUF2. PUF2 of dm CTD was closer in energy to the N state of dm CTD than PUF2 of wt CTD to the N state of wt CTD: PUF2 of dm CTD showed significantly higher dynamics in the C-terminal region of $\alpha 1$, in $\beta 2$ and in the central region of $\alpha 3$, when compared to PUF2 of wt CTD (Table 1). Previously, PUF1 had been shown to possess a dynamic or disordered $\beta 1$ and dynamic N and C termini of both $\alpha 2$ and $\alpha 3$, in the case of wt CTD. In the case of dm CTD, the $\beta 1$ region showed a significant increase in dynamics in PUF1.

A previous study [6] had shown that PUF2 formed by wt CTD was 3.1 kcal mol⁻¹ less stable than the N state. For dm CTD, PUF2 was found to be 2.7 kcal mol⁻¹ less stable than the N state. The stability ($\Delta G_{op} = 2.7 \pm 0.4$ kcal mol⁻¹) and accessible surface area change in PUF2 ($m_{op} = 0.6 \pm 0.05$ kcal mol⁻¹ M⁻¹) with respect to the N state were identical to the values of ΔG_{IN}^0 (2.7 kcal mol⁻¹), the free energy of change from N to I, and m_{IN} (0.6 kcal mol⁻¹ M⁻¹), the measure of the change in accessible surface area from N to I. These similarities suggested that PUF2 is the monomeric precursor that initiates misfolding, resulting in oligomerization.

Discussion

In the search for conformations that are prone to misfolding and aggregation, native PrP has been perturbed, destabilized, or completely unfolded by chemical denaturants, temperature, pressure, pH, and mutations [10,35–41]. Studies on the folding pathways of pathogenic variants of different PrPs have identified obligatory intermediates populated during the folding of these proteins. The extents to which these intermediates are populated have been observed to be directly related to the pathogenicity of these proteins [31]. However, structural information on such intermediates has been unavailable. In equilibrium unfolding studies, NMR has detected a few partially structured states for human PrP [38] and a continuum of intermediates for other prion variants [42]. A direct role of any of these intermediates in initiating aggregation was, however, not shown.

Mutation of F174 to Trp stabilizes a monomeric equilibrium intermediate at low pH

In dm CTD, the buried Phe174 was replaced by Trp, and the solvent-exposed Trp144 by Phe. The stability of the N state was found to be not affected; it appears that any stabilization caused by introducing the more hydrophobic Trp into the protein core is offset by the destabilization caused by steric strain introduced in replacing the smaller Phe by the larger Trp in the core. In the intermediate I, it appears that less such destabilization occurs, presumably because I is not as well-packed as N. Consequently, there is net stabilization of I, and it is populated significantly at equilibrium. It should be noted that the second mutation in dm CTD, the replacement of the solvent-exposed W144 by the smaller, less hydrophobic Phe is not expected [43] to be disruptive to the protein (Fig. 1b). In this study of unfolding at low pH in the absence of salt, the intermediate (I) populated during the urea-induced unfolding transition of dm CTD was found to be monomeric (see Results). In contrast, previous studies on wt CTD in the presence of salt at low pH had indicated that an equilibrium intermediate is populated but that the intermediate is octameric [16,44,45]. The observation that the stability of the equilibrium intermediate, I, is identical to that of PUF2, as determined from HDX-MS studies of dm CTD and wt CTD, suggested that I is PUF2. Moreover, PUF2 and I have similar structural characteristics. The urea-induced equilibrium unfolding study suggests that I has an unfolded-like secondary structure (see Results). The HDX-MS study showed that with the exception of the disulfide-bonded region, the rest of the protein in PUF2 is unprotected, likely due to a loss in secondary structure. Since W174, which is the

fluorescence probe used in this study, is proximal to the disulfide-bonded core that is still structured in PUF2, I also appeared to show N-like tertiary structural properties.

Misfolding initiates from PUF2/I

The observations that the rate of misfolding is fastest at the urea concentration (~4 M) where PUF2/I is maximally populated (Fig. 3b) and that the rate of misfolding is directly and linearly dependent on the concentration of PUF2/I strongly suggest that misfolding commences from PUF2/I. Under the experimental conditions (150 mM NaCl at 25 °C and at pH 4, in the presence of varying urea concentrations) used to misfold moPrP in this study, misfolding is known to be accompanied by oligomerization [29]. The observation that the reaction order for the misfolding reaction is 2.45 (Fig. S3) suggests that the misfolding reaction is association-limited with respect to the concentration of I [46]. The observation of a reaction order of ~2 rules out the possibility of a slow, rate-limiting conversion of I to another conformation (I*) from which oligomer formation proceeds. It would appear that the oligomerization process is limited by the direct association of I to aggregate or that oligomerization proceeds *via* a fast conformational conversion to I* followed by a slow, rate-limiting association of I* to aggregate [47].

It should be noted that although it has been assumed here that urea changes only the stability and hence the population of I, the effect of urea on the stability of the oligomers formed is not known. However, since the oligomers formed by dm CTD at different urea concentrations are structurally similar (by CD) and have the same size (by DLS), these oligomers appear to have the same stability to urea, unlike oligomers formed under other conditions. Moreover, the rate-limiting step in the oligomerization of dm CTD is the dimerization of the monomer and does not involve the formation of the oligomer. Also, the linear dependence of k_{app} on the fractional population of monomeric I (Fig. 3c) is suggestive of the fact that the stability of the dimer does not play a significant role in determining the rate of oligomerization, likely because the dimer is immediately recruited for further growth after the rate-limiting step.

The structure of PUF2/I and the initiation of misfolding

The HDX-MS results suggest that sequence stretch 127–146 and the N and C termini of $\alpha 2$ and $\alpha 3$ are solvent-exposed in PUF2/I, as a result of either increased dynamics or fraying of secondary structure in these regions. In this regard, PUF2/I resembles an intermediate detected by NMR during the denaturant-induced unfolding of the human PrP

[38]. However, PUF2 shows, additionally, solvent-exposed $\alpha 1$ and $\beta 2$ regions. $\alpha 1$ is one of the most hydrophilic helices in any protein in the PDB [48] and is stabilized primarily by internal salt bridges. It is docked against the hydrophobic $\alpha 2$ – $\alpha 3$ core by a few long-range “anchoring” interactions with residues in $\alpha 2$ and $\alpha 3$ [49]. Although initial studies had indicated that the highly stable $\alpha 1$ was unlikely to be involved in initiating misfolding [50] and was likely to be structured in monomeric, aggregation-prone PrP intermediates [10], the loss of stabilizing salt-bridge interactions in $\alpha 1$ was shown to promote misfolding [51]. More recent studies have suggested that the separation of the $\alpha 1$ – $\beta 2$ subdomain from the aggregation-prone $\alpha 2$ – $\alpha 3$ core [52,53] is a crucial step in initiating misfolding at both low [54] and physiological pH [55]. Indeed, pathogenic mutations have been observed to facilitate the separation of these two subdomains by increasing the dynamics at the $\alpha 1$ – $\beta 2$ and $\beta 2$ – $\alpha 2$ loop shown in both experimental [56–58] and computational studies [49,59–62]. However, the extent to which structural changes in monomeric PrP are required to initiate misfolding remains ambiguous.

Molten globule (MG)-like conformers, wherein the $\alpha 1$ – $\beta 2$ subdomain was detached from the $\alpha 2$ – $\alpha 3$ core, have been observed to populate at extremely low pH [11,13] (referred to as the A state) and also upon mutagenesis at the hydrophobic core [12]. These conformations were much more structured at the $\alpha 2$ – $\alpha 3$ core and in the loop regions (154–160 and 199–202) than I/PUF2 identified in the current study. In the previous studies, these highly structured MG forms had been implicated to be the species that initiated aggregation [11–13], on the basis of the observation that the logarithm of the misfolding rate was linearly dependent on the logarithm of the MG concentration, but it should be noted that such a log–log linear dependence will be seen for any partially unfolded conformer populated in equilibrium with the species from which aggregation actually begins. Thus, the previous studies [11–13] did not rigorously demonstrate that the MG forms directly initiated aggregation. In contrast, the current study shows that the rate of misfolding is directly proportional to the concentration of PUF2/I present and that the misfolding and oligomerization are limited by the dimerization of I. Hence, the current study shows that the previously identified MG forms do not misfold directly but must first unfold further in order for misfolding to be able to commence.

In the case of dm CTD, I/PUF2 is stable over time, but misfolds and oligomerizes rapidly upon the addition of salt. It is likely that the salt screens the electrostatic repulsion between hydrophilic, charged residues of two proximal I molecules, which prevents them from aggregating. It remains to be shown whether, in addition to this general screening of salt

that would facilitate aggregation, whether there is also a specific structural perturbation affected by salt, which triggers the cascade of unfolding events leading ultimately to the formation of I/PUF2 and consequent misfolding and aggregation.

From the structural information obtained on the aggregation-prone PUF2/I, the effects of pathogenic mutations on the population of the intermediate may be gauged. Pathogenic mutations may or may not affect the N state stability. Perturbations of key salt-bridge or hydrophobic interactions between residues in the N state, which are either absent or present partially in PUF2/I, are expected to selectively destabilize N relative to PUF2/I [63], resulting in an increase in population of I. For example, pairwise interactions between residues, such as D177-R163/Y127, T182-Y161, D201-R155, and H186-R155, which are known to anchor $\alpha 1$ against $\alpha 2$ – $\alpha 3$, or packing interactions of Q216 in the hydrophobic core of the protein, stabilize the N state [49]. These interactions can be disrupted either by protonation or deprotonation of residues by a change in pH [64–66] or as a result of pathogenic mutations (D177N, T182A, D201N, R207H, and Q216R). Such perturbations result not only in destabilization of the N state [67] but also in increased dynamics in $\alpha 1$ and $\beta 2$ [12,57] and in an increase in the PUF2/I population, owing to a decrease in the energy difference between N and PUF2/I. On the other hand, mutations that stabilize N [29,68] or destabilize PUF2/I relative to U show a decrease in the aggregation propensity, as PUF2/I becomes energetically less accessible from the N state. In general, it seems that any mutation, pathogenic or non-pathogenic, which increases the probability of populating PUF2/I either by selectively destabilizing the N state or by stabilizing PUF2/I relative to U, increases the propensity of the protein to misfold.

The current study indicates that the presence of the N-terminal region is not necessary for the formation of the intermediate, I, although the association of I to oligomers, or the conversion to fibrils, might be effected. The N-terminal unstructured region may have transient interactions with the globular domain promoting aggregation indirectly, as observed in the case of acylphosphatase, where transient interactions of the N-terminal unstructured region with the globular domain promoted the assembly process [69].

It is also known that the PrP forms toxic oligomers at low pH under solvent conditions identical to that used in the current study [16,44] suggesting that the oligomers formed in this study are also cytotoxic. Moreover, oligomers formed under such solvent conditions have been shown to possess physicochemical properties of PrP^{Sc} [70]. Indeed, the oligomers formed by the dm CTD were observed to be partially resistant to proteinase K (Fig. S5).

Conclusion

Introduction of a tryptophan residue into the hydrophobic core of the CTD of moPrP stabilizes and populates a high energy intermediate, I, during unfolding. I is monomeric and has secondary structural properties similar to that of the U state, while its fluorescence properties are similar to that of the N state. I can be identified, energetically and structurally, as a PUF of the protein, PUF2, revealed by a native-state HDX-MS study. I/PUF2 is less structured than the highly structured MG forms thought previously to initiate aggregation [11–13]. The current study shows, however, that the structured MG forms must unfold further to I/PUF2 before misfolding can commence. It appears that it is I/PUF2 that directly initiates misfolding, as the rate of misfolding was found to be directly proportional to the concentration of PUF2/I present, and misfolding and oligomerization are limited by the dimerization of I.

This study shows how aggregation-prone high energy intermediates may be structurally characterized by low-resolution probes, after specifically stabilizing them using mutagenesis. By determining the complete extent of native structure that is required to be lost before misfolding and aggregation can begin, this study also provides a general mechanism describing how the misfolding of PrP is initiated, which may be used to predict and explain the effect of different mutations on the aggregation propensity of PrP.

Materials and Methods

Site-directed mutagenesis

The plasmid (pPrP-C) encoding the gene for wt CTD, moPrP (121–231), was a gift from Prof. R. Glockshuber. The W144F mutation was first generated by site-directed mutagenesis of wt CTD, after which the F174W mutation was generated. Primers were obtained from Sigma. The mutations in the plasmid were confirmed by DNA sequencing.

Protein expression and purification

The double mutant variant W144F/F174W moPrP (121–231) is henceforth referred to as dm CTD. wt CTD and dm CTD were expressed in *Escherichia coli* BL21(DE3) codon plus cells (Stratagene) and grown initially at 37 °C. After the optical density at 600 nm reached 1.2, IPTG induction at a final concentration of 1 mM was done, and the cells were grown at 25 °C overnight. After centrifugation, the proteins were extracted from the periplasmic fraction

using 500 mM sucrose in 200 mM Tris–HCl and 5 mM EDTA at pH 8 and purified as described previously [71]. The proteins were dialyzed against 0.22- μ m filtered water and stored at –80 °C. The concentration of wt CTD was determined by absorbance measurements at 280 nm, using an extinction coefficient of 19890 M⁻¹ cm⁻¹ [67]. For dm CTD, the molar extinction coefficient was estimated, from the absorbance spectra of native and denatured dm CTD in 6 M GdnHCl [72], to be 20686 M⁻¹ cm⁻¹. The purity of each protein was confirmed by SDS-PAGE and mass spectrometry using a Waters Synapt G2 mass spectrometer. The proteins were found to be >95% pure. Both the proteins had a mass of 13,334 Da, as expected.

Chemicals and buffers

The chemicals used in this study were obtained from Sigma, unless mentioned otherwise. For experiments that were carried out at pH 4, native buffer containing 20 mM sodium acetate and unfolding buffer containing 20 mM sodium acetate with variable concentrations of urea (obtained from United States Biochemical Corporation) in the range 0–10 M were used. For experiments that were carried out at pH 7, native buffer containing 50 mM sodium phosphate and unfolding buffer containing 50 mM sodium phosphate along with variable concentrations of urea in the range 0–10 M were used. All solutions were filtered using 0.22- μ m Millipore syringe filters before use. The concentrations of urea stock solutions were determined, prior to use, by refractive index measurements using an Abbe refractometer.

Far-UV CD spectra of wt CTD and dm CTD at 25 °C

Far-UV CD spectra of native and unfolded wt CTD and dm CTD at pH 4 were acquired on a Jasco J-815 spectropolarimeter using a protein concentration of 10 μ M in a 0.1-cm path length cuvette, with a bandwidth of 1 nm, a scan speed of 50 nm/min, and a digital integration time of 1 s.

Fluorescence spectra of dm CTD at 25 °C

Fluorescence spectra of native and unfolded dm CTD at pH 4 were collected using excitation wavelengths of 280 nm and 295 nm on a Fluoromax 3 fluorimeter (Horiba), using a protein concentration of 5 μ M in a 1-cm path length cuvette, with an excitation bandwidth of 1 nm and an emission bandwidth of 5 nm.

Urea-induced denaturation

To monitor secondary structural changes upon urea-induced unfolding of dm CTD at 25 °C, far-UV

CD measurements were carried out at 222 nm on a Jasco J-815 spectropolarimeter. A 0.1 cm path length cuvette was used for the measurements, with a bandwidth of 1 nm and a digital integration time of 1 s. The signal for each sample was averaged for 1 min. The sample temperature was maintained by a Peltier temperature controller (PTC-423L) from Jasco.

The tertiary structural changes upon urea-induced unfolding at 25 °C were monitored by fluorescence measurements on a MOS 450 optical system from Biologic using excitation wavelengths of both 280 nm and 295 nm, and the emission was collected at 360 nm using a 10 nm bandpass filter (Asahi Spectra). The path length of the cuvette used was 1 cm.

For both these measurements, the protein concentrations used were in the range 5–50 μM, and the samples in different concentrations of urea were incubated for 3 h at 25 °C, to ensure that equilibrium was reached, before the measurements were carried out.

Data analysis

The urea-induced unfolding transitions monitored by mean residual ellipticity and fluorescence measurements were converted to apparent fraction unfolded, f_{app} , plots as described previously [5]. For a three-state model, $N \leftrightarrow I \leftrightarrow U$, which incorporates one intermediate, I, f_{app} is given by Eq. (1) [26].

$$f_{app} = \frac{Z \cdot K_{IN} + K_{IN} \cdot K_{UI}}{[1 + K_{IN} + K_{IN} \cdot K_{UI}]} \quad (1)$$

Here, K_{IN} and K_{UI} are the apparent equilibrium constants for the N-to-I and I-to-U transitions. Z is the fractional signal for I given by Eq. (2), where S_I , S_N , and S_U are the signals of I, N, and U, respectively.

$$Z = \frac{S_I - S_N}{S_U - S_N} \quad (2)$$

K_{IN} and K_{UI} are related to the free energy changes, ΔG_{IN}^0 and ΔG_{UI}^0 by Eqs. (3a) and (3b). R is the universal gas constant, D is denaturant concentration, and T is the temperature.

$$K_{IN} = \exp\left[-\frac{\Delta G_{IN}^0 + m_{IN}[D]}{RT}\right] \quad (3a)$$

$$K_{UI} = \exp\left[-\frac{\Delta G_{UI}^0 + m_{UI}[D]}{RT}\right] \quad (3b)$$

The fractional population of each thermodynamic state, f_N , f_I , and f_U is given by:

$$f_N = \frac{1}{1 + K_{IN} + K_{UI} K_{IN}} \quad (4a)$$

$$f_I = \frac{K_{IN}}{1 + K_{IN} + K_{UI} K_{IN}} \quad (4b)$$

$$f_U = \frac{K_{UI} K_{IN}}{1 + K_{IN} + K_{UI} K_{IN}} \quad (4c)$$

The values of ΔG_{IN}^0 and ΔG_{UI}^0 , the free energy changes for the N-to-I and I-to-U transitions, respectively, and their dependences on denaturant concentrations, m_{IN} and m_{UI} , respectively, were obtained by globally fitting the denaturant dependences of f_{app} to Eq. (1), using a MATLAB® [73] program. These values have been reported as mean \pm SD obtained from three independent experiments (see Results).

Misfolding and oligomerization of dm CTD

For studying the misfolding of dm CTD at pH 4, 50 μM dm CTD was incubated in 20 mM sodium acetate in the presence of varying concentrations of urea in the range 0–6 M for 3 h at 25 °C. The misfolding reaction was initiated by the addition of NaCl to a final concentration of 150 mM to the above reaction mixtures containing different urea concentrations. The dead time of mixing for all measurements was 1.1 min. The change in secondary structure was monitored at 215 nm on a Jasco J-815 spectropolarimeter, immediately after the initiation of misfolding, using a 0.1 cm path length cuvette. A bandwidth of 1 nm and a digital integration time of 32 s were used. The percentage misfolding of dm CTD was calculated using Eq. (5), as shown below:

$$\% \text{ Misfolding} = \frac{(S_t - S_0)}{(S_f - S_0)} \times 100 \quad (5)$$

Here, S_t is the signal at 215 nm at time, t , after initiation of misfolding. S_0 is the signal at 0 h and S_f is the signal after saturation of the misfolding and oligomerization reaction. Far-UV CD spectra of dm CTD were acquired before the initiation of each misfolding reaction. In order to obtain the rate of misfolding and oligomerization, the % Misfolding kinetic traces were fit to either Eq. (6a) or (6b).

$$\% \text{ Misfolding} (t) = y_0 + a(1 - e^{-k_1 t}) \quad (6a)$$

$$\% \text{ Misfolding } (t) = y_0 + a(1 - e^{-k_1 t}) + b(1 - e^{-k_2 t}) \quad (6b)$$

Here, y_0 is the % Misfolding at 0 h, and a and b are the relative amplitudes of the fast and slow phases whose rates are given by k_1 and k_2 , respectively. The mean misfolding and oligomerization rate, k_{app} , is given by:

$$k_{app} = \frac{1}{\left(\frac{\alpha^1}{k_1}\right) + \left(\frac{\alpha^2}{k_2}\right)} \quad (6c)$$

In Eq. (6c), α_1 and α_2 are the fractional amplitudes of the fast and slow phases. At the end of the misfolding and oligomerization reactions in different concentrations of urea, when the CD signal at 215 nm had saturated, far-UV CD spectra of the oligomers were collected using a 0.1 cm path length cuvette, a bandwidth of 1 nm, a scan speed of 50 nm/min, and a digital integration time of 1 s.

Native-state HDX-MS of wt CTD and dm CTD

The peptide maps of wt CTD and dm CTD were generated, and HDX-MS measurements were carried out, as described previously [6]. Since the results from HDX-MS of wt CTD were identical to those obtained with the CTD region of wt moPrP (23–231; data not shown), the residues exchanging in the slow phase of exchange were assumed to be identical to those in moPrP (23–231). Hence, the intrinsic rate of exchange for each peptide segment was considered to be the same as that reported previously for moPrP (23–231) [6]. The stability of each sequence segment was evaluated as described before [6]. The dependences of stabilities of the different sequence segments of dm CTD on urea were determined as described before [6].

Acknowledgment

We thank M.K. Mathew, R. Varadarajan, and members of our laboratory for discussions. J.B.U. is a recipient of a JC Bose National Fellowship from the Government of India. This work was funded by the Tata Institute of Fundamental Research and by the Department of Biotechnology, Government of India.

Conflict of interest: The authors declare that they have no conflict of interest with the contents of this article.

Appendix A. Supplementary Data

Supplementary data to this article can be found online at <http://dx.doi.org/10.1016/j.jmb.2017.01.019>.

Received 6 December 2016;
Received in revised form 19 January 2017;
Accepted 19 January 2017
Available online 29 January 2017

Keywords:

partially unfolded forms;
prion;
hydrogen–deuterium exchange;
mass spectrometry;
misfolding

Abbreviations used:

PrP, prion protein; PrP^C, cellular PrP; PrP^{Sc}, scrapie PrP; HDX, hydrogen–deuterium exchange; moPrP, mouse PrP; PUF, partially unfolded form; CTD, C-terminal domain; dm CTD, double mutant variant of the C-terminal domain; wt, wild-type; DLS, dynamic light scattering; HDX-MS, HDX-nuclear magnetic resonance spectroscopy; ANS, 1-anilino-8-naphthalene sulfonate.

References

- [1] S.B. Prusiner, Molecular biology of prion diseases, *Science* 252 (1991) 1515–1522.
- [2] R.G. Will, M.P. Alpers, D. Dormont, L.B. Schonberger, Infectious and Sporadic Prion diseases, in: S.B. Prusiner (Ed.), *Prion Biology and Diseases*, 2004 (Second Edition; Chapter: 13).
- [3] H. Zhang, J. Sto, I. Mehlhorn, D. Groth, M.A. Baldwin, S.B. Prusiner, T.L. James, F.E. Cohen, Physical studies of conformational plasticity in a recombinant prion protein, *Biochemistry* 36 (1997) 3543–3553.
- [4] C. Soto, Prion hypothesis : the end of the controversy? *Trends Biochem. Sci.* 36 (2011) 151–158.
- [5] R. Moulick, J.B. Udgaonkar, Thermodynamic characterization of the unfolding of the prion protein, *Biophys. J.* 106 (2014) 410–420.
- [6] R. Moulick, R. Das, J.B. Udgaonkar, Partially unfolded forms of the prion protein populated under misfolding-promoting conditions, *J. Biol. Chem.* 290 (2015) 25,227–25,240.
- [7] F. Chiti, C.M. Dobson, Amyloid formation by globular proteins under native conditions, *Nat. Chem. Biol.* 5 (2009) 15–22.
- [8] A. De Simone, A. Dhulesia, G. Soldi, M. Vendruscolo, S.D. Hsu, F. Chiti, C.M. Dobson, Experimental free energy surfaces reveal the mechanisms of maintenance of protein solubility, *Proc. Natl. Acad. Sci.* 108 (2011) 21,057–21,062.
- [9] F.E. Cohen, K.M. Pan, Z. Huang, M. Baldwin, R.J. Fletterick, S.B. Prusiner, Structural clues to prior replication, *Science* 264 (1994) 530–531.

- [10] K. Kuwata, H. Li, H. Yamada, G. Legname, S.B. Prusiner, K. Akasaka, T.L. James, Locally disordered conformer of the hamster prion protein: a crucial intermediate to PrP^{Sc}? *Biochemistry* 41 (2002) 12,277–12,283.
- [11] R.P. Honda, K. Yamaguchi, K. Kuwata, Acid-induced molten globule state of a prion protein: crucial role of strand 1-helix 1-strand 2 segment, *J. Biol. Chem.* 289 (2014) 30,355–30,363.
- [12] J. Singh, J.B. Udgaonkar, The pathogenic mutation T182A converts the prion protein into a molten globule-like conformation whose misfolding to oligomers but not to fibrils is drastically accelerated, *Biochemistry* 55 (2016) 459–469.
- [13] R.P. Honda, M. Xu, K. Yamaguchi, H. Roder, K. Kuwata, A native-like intermediate serves as a branching point between the folding and aggregation pathways of the mouse prion protein, *Structure* 23 (2015) 1–8.
- [14] G.S. Jackson, A.F. Hill, C. Joseph, L. Hosszu, A. Power, J.P. Waltho, A.R. Clarke, J. Collinge, Multiple folding pathways for heterologously expressed human prion protein, *Biochem. Biophys. Acta* 1431 (1999) 1–13.
- [15] R. Gerber, A. Tahiri-Alaoui, P.J. Hore, W. James, Conformational pH dependence of intermediate states during oligomerization of the human prion protein, *Protein Sci.* 17 (2008) 537–544.
- [16] M.Q. Khan, B. Sweeting, V.K. Mulligan, P.E. Arslan, N.R. Cashman, E.F. Pai, A. Chakrabarty, Prion disease susceptibility is affected by β -structure folding propensity and local side-chain interactions in PrP, *Proc. Natl. Acad. Sci.* 107 (2010) 19,808–19,813.
- [17] D.M. Korzhnev, L.E. Kay, Protein molecules by relaxation dispersion NMR spectroscopy: an application to protein folding, *Acc. Chem. Res.* 41 (2008) 442–451.
- [18] K. Sridevi, J.B. Udgaonkar, Unfolding rates of barstar determined in native and low denaturant conditions indicate the presence of intermediates, *Biochemistry* 41 (2002) 1568–1578.
- [19] P. Malhotra, J.B. Udgaonkar, High-energy intermediates in protein unfolding characterized by thiol labeling under natively like conditions, *Biochemistry* 53 (2014) 3608–3620.
- [20] Y. Bai, T.R. Sosnick, L. Mayne, S.W. Englander, Protein folding intermediates: native state hydrogen exchange, *Science* 269 (1995) 192–197.
- [21] A.K. Chamberlain, T.M. Handel, S. Marqusee, Detection of rare partially folded molecules in equilibrium with the native conformation of RNaseH, *Nat. Struct. Biol.* 3 (1996) 782–787.
- [22] Y.J.M. Bollen, M.B. Kamphuis, C.P.M. van Mierlo, The folding energy landscape of apoflavodoxin is rugged: hydrogen exchange reveals nonproductive misfolded intermediates, *Proc. Natl. Acad. Sci.* 103 (2006) 4095–4100.
- [23] L.L.P. Hosszu, N.J. Baxter, S. Graham, G.S. Jackson, A. Power, A.R. Clarke, J.P. Waltho, C.J. Craven, J. Collinge, Structural mobility of the human prion protein probed by backbone hydrogen exchange, *Nat. Struct. Biol.* 6 (1999) 740–743.
- [24] E.M. Nicholson, H. Mo, S.B. Prusiner, F.E. Cohen, S. Marqusee, Differences between the prion protein and its homolog doppel: a partially structured state with implications for scrapie formation, *J. Mol. Biol.* 1 (2002) 807–815.
- [25] M. Ikeguchi, K. Kuwajima, M. Mitani, S. Sugai, Evidence for identity between the equilibrium unfolding intermediate and a transient folding intermediate: a comparative study of the folding reactions of α -lactalbumin and lysozyme, *Biochemistry* 25 (1986) 6965–6972.
- [26] D. Barrick, R.L. Baldwin, Three-state analysis of sperm whale apomyoglobin folding, *Biochemistry* 32 (1993) 3790–3796.
- [27] J. Zitzewitz, C.R. Matthews, Protein engineering strategies in examining protein folding intermediates, *Curr. Opin. Struct. Biol.* 3 (1993) 594–600.
- [28] J.M. Sanz, A.R. Fersht, Rationally designing the accumulation of a folding intermediate of barnase by protein engineering, *Biochemistry* 32 (1993) 13,584–13,592.
- [29] J. Singh, H. Kumar, A.T. Sabareesan, J.B. Udgaonkar, Rational stabilization of helix 2 of the prion protein prevents its misfolding and oligomerization, *J. Am. Chem. Soc.* 136 (2014) 16,704–16,707.
- [30] G. Wildegger, S. Liemann, R. Glockshuber, Extremely rapid folding of the C-terminal domain of the prion protein without kinetic intermediates, *Nat. Struct. Biol.* 6 (1999) 550–553.
- [31] A.C. Apetri, K. Surewicz, W.K. Surewicz, The effect of disease-associated mutations on the folding pathway of human prion protein, *J. Biol. Chem.* 23 (2004) 18,008–18,014.
- [32] R.W. Cowgill, Fluorescence and protein structure: XI. Fluorescence quenching by disulfide and sulfhydryl groups, *Biochim. Biophys. Acta* 140 (1967) 37–44.
- [33] K.P. Wong, C. Tanford, Denaturation of bovine carbonic anhydrase B by guanidine hydrochloride, *J. Biol. Chem.* 248 (1973) 8518–8523.
- [34] R. Gerber, A. Tahiri-Alaoui, P.J. Hore, W. James, Oligomerization of the human prion protein proceeds via a molten globule intermediate, *J. Biol. Chem.* 282 (2007) 6300–6307.
- [35] J.H. Viles, D. Donne, G. Kroon, S.B. Prusiner, F.E. Cohen, H.J. Dyson, P.E. Wright, Local structural plasticity of the prion protein. Analysis of NMR relaxation dynamics, *Biochemistry* 40 (2001) 2743–2753.
- [36] A.C. Apetri, W.K. Surewicz, Kinetic intermediate in the folding of human prion protein, *J. Biol. Chem.* 277 (2002) 44,589–44,592.
- [37] S.M. Martins, A. Chapeaurouge, S.T. Ferreira, Folding intermediates of the prion protein stabilized by hydrostatic pressure and low temperature, *J. Biol. Chem.* 278 (2003) 50,449–50,455.
- [38] L.L.P. Hosszu, M.A. Wells, G.S. Jackson, S. Jones, M. Batchelor, A.R. Clarke, C.J. Craven, J.P. Waltho, J. Collinge, Definable equilibrium states in the folding of human prion protein, *Biochemistry* 44 (2005) 16,649–16,657.
- [39] N. Kachel, W. Kremer, R. Zahn, H.R. Kalbitzer, Observation of intermediate states of the human prion protein by high pressure NMR spectroscopy, *BMC Struct. Biol.* 6 (2006) 16.
- [40] A.C. Apetri, K. Maki, H. Roder, W.K. Surewicz, Early intermediate in human prion protein folding as evidenced by ultrarapid mixing experiments, *J. Am. Chem. Soc.* 128 (2006) 11,673–11,678.
- [41] T. Hart, L.L.P. Hosszu, C.R. Trevitt, G.S. Jackson, J.P. Waltho, J. Collinge, A.R. Clarke, Folding kinetics of the human prion protein probed by temperature jump, *Proc. Natl. Acad. Sci.* 106 (2009) 5651–5656.
- [42] O. Julien, S. Chatterjee, T.C. Bjorndahl, B. Sweeting, S. Acharya, V. Semenchenko, A. Chakrabarty, E.F. Pai, D.S. Wishart, B.D. Sykes, N.R. Cashman, Relative and regional stabilities of the hamster, mouse, rabbit, and bovine prion proteins toward urea unfolding assessed by nuclear magnetic resonance and circular dichroism spectroscopies, *Biochemistry* 50 (2011) 7536–7545.
- [43] T. Alber, D.P. Sun, J.A. Nye, D.C. Muchmore, B.W. Matthews, Temperature-sensitive mutations of bacteriophage T4 lysozyme occur at sites with low mobility and low solvent accessibility in the folded protein, *Biochemistry* 26 (1987) 3754–3758.

- [44] S. Homemann, R. Glockshuber, A scrapie-like unfolding intermediate of the prion protein domain PrP(121-231) induced by acidic pH, *Proc. Natl. Acad. Sci.* 95 (1998) 6010–6014.
- [45] I.V. Baskakov, G. Legname, S.B. Prusiner, F.E. Cohen, Folding of prion protein to its native α -helical conformation is under kinetic control, *J. Biol. Chem.* 276 (2001) 19,687–19,690.
- [46] C.J. Roberts, Kinetics of irreversible protein aggregation: analysis of extended Lumry-Eyring models and implications for predicting protein shelf life, *J. Phys. Chem. B* 107 (2003) 1194–1207.
- [47] C.J. Roberts, Nonnative Protein Aggregation, in: R. Murphy, A.M. Tsai (Eds.), *Misbehaving Proteins: Protein (Mis) Folding, Aggregation and Stability*, Edition 1 Springer, New York 2006, pp. 17–46 Chapter: 2.
- [48] M.P. Morrissey, E.I. Shakhnovich, Evidence for the role of PrP C helix 1 in the hydrophilic seeding of prion aggregates, *Proc. Natl. Acad. Sci.* 96 (1999) 11,293–11,298.
- [49] A. De Simone, A. Zagari, P. Derreumaux, Structural and hydration properties of the partially unfolded states of the prion protein, *Biophys. J.* 93 (2007) 1284–1292.
- [50] J. Ziegler, H. Sticht, U.C. Marx, W. Müller, P. Rösch, S. Schwarzingler, CD and NMR studies of prion protein (PrP) helix 1: Novel implications for its role in the PrPC→PrPSc conversion process, *J. Biol. Chem.* 278 (2003) 50,175–50,181.
- [51] J.O. Speare, T.S. Rush, M.E. Bloom, B. Caughey, The role of helix 1 aspartates and salt bridges in the stability and conversion of prion protein, *J. Biol. Chem.* 278 (2003) 12,522–12,529.
- [52] M. Gasset, M.A. Baldwin, D.H. Lloyd, J.M. Gabriel, D.M. Holtzman, F. Cohen, R. Fletterick, S.B. Prusiner, Predicted alpha-helical regions of the prion protein when synthesized as peptides form amyloid, *Proc. Natl. Acad. Sci.* 89 (1992) 10,940–10,944.
- [53] N. Chakroun, S. Prigent, C.A. Dreiss, S. Noinville, C. Chapuis, F. Fraternali, H. Rezaei, The oligomerization properties of prion protein are restricted to the H2H3 domain, *FASEB J.* 24 (2010) 3222–3231.
- [54] F. Eghiaian, T. Daubenfeld, Y. Quenet, M. van Audenhaege, A.P. Bouin, G. van der Rest, J. Grosclaude, H. Rezaei, Diversity in prion protein oligomerization pathways results from domain expansion as revealed by hydrogen/deuterium exchange and disulfide linkage, *Proc. Natl. Acad. Sci.* 104 (2007) 7414–7419.
- [55] I. Hafner-Bratkovič, R. Bester, P. Pristovšek, L. Gaedtke, P. Veranič, J. Gašperšič, M. Manček-Keber, M. Avbelj, M. Polymenidou, C. Julius, A. Aguzzi, I. Vorberg, R. Jerala, Globular domain of the prion protein needs to be unlocked by domain swapping to support prion protein conversion, *J. Biol. Chem.* 286 (2011) 12,149–12,156.
- [56] S. Hadži, A. Ondračka, R. Jerala, I. Hafner-Bratkovič, Pathological mutations H187R and E196K facilitate subdomain separation and prion protein conversion by destabilization of the native structure, *FASEB J.* 29 (2015) 882–893.
- [57] J. Singh, J.B. Udgaonkar, Structural effects of multiple pathogenic mutations suggest a model for the initiation of misfolding of the prion protein, *Angew. Chem.* 54 (2015) 7529–7533.
- [58] I. Biljan, G. Ilc, G. Giachin, J. Plavec, G. Legname, Structural rearrangements at physiological pH: nuclear magnetic resonance insights from the V210I human prion protein mutant, *Biochemistry* 51 (2012) 7465–7474.
- [59] M.L. DeMarco, V. Daggett, Molecular mechanism for low pH triggered misfolding of the human prion protein, *Biochemistry* 46 (2007) 3045–3054.
- [60] S.R.R. Campos, M. Machuqueiro, A.M. Baptista, Constant-pH molecular dynamics simulations reveal a β -rich form of the human prion protein, *J. Phys. Chem. B* (2010) 12,692–12,700.
- [61] M.W. van der Kamp, V. Daggett, Influence of pH on the human prion protein: Insights into the early steps of misfolding, *Biophys. J.* 99 (2010) 2289–2298.
- [62] W. Chen, M.W. van der Kamp, V. Daggett, Structural and dynamic properties of the human prion protein, *Biophys. J.* 106 (2014) 1152–1163.
- [63] D. Canet, M. Sunde, A.M. Last, A. Miranker, A. Spencer, C.V. Robinson, C.M. Dobson, Mechanistic studies of the folding of human lysozyme and the origin of amyloidogenic behavior in its disease-related variants, *Biochemistry* 38 (1999) 6419–6427.
- [64] E. Langella, R. Improta, V. Barone, Checking the pH-induced conformational transition of prion protein by molecular dynamics simulations: effect of protonation of histidine residues, *Biophys. J.* 87 (2004) 3623–3632.
- [65] S.H. Bae, G. Legname, A. Serban, S.B. Prusiner, P.E. Wright, H.J. Dyson, Prion proteins with pathogenic and protective mutations show similar structure and dynamics, *Biochemistry* 48 (2009) 8120–8128.
- [66] J. Singh, J.B. Udgaonkar, Unraveling the molecular mechanism of pH-induced misfolding and oligomerization of the prion protein, *J. Mol. Biol.* 428 (2016) 1–11.
- [67] S. Liemann, R. Glockshuber, Influence of amino acid substitutions related to inherited human prion diseases on the thermodynamic stability of the cellular prion protein, *Biochemistry* 38 (1999) 3258–3267.
- [68] Q. Kong, J.L. Mills, B. Kundu, X. Li, L. Qing, K. Surewicz, I. Cali, S. Huang, M. Zheng, W. Swietnicki, F.D. Sönnichsen, P. Gambetti, W.K. Surewicz, Thermodynamic stabilization of the folded domain of prion protein inhibits prion infection *in vivo*, *Cell Rep.* 4 (2013) 248–254.
- [69] G. Plakoutsi, F. Bemporad, M. Monti, D. Pagnozzi, P. Pucci, F. Chiti, Exploring the mechanism of formation of native-like and precursor amyloid oligomers for the native acylphosphatase from *Sulfolobus solfataricus*, *Structure* 14 (2006) 993–1001.
- [70] W. Swietnicki, M. Morillas, S.G. Chen, P. Gambetti, W.K. Surewicz, Aggregation and fibrillization of the recombinant human prion protein, *Biochemistry* 39 (2000) 424–431.
- [71] S. Homemann, R. Glockshuber, Autonomous and reversible folding of a soluble amino-terminally truncated segment of the mouse prion protein, *J. Mol. Biol.* 261 (1996) 614–619.
- [72] S.C. Gill, P.H. von Hippel, Calculation of protein extinction coefficients from amino acid sequence data, *Anal. Biochem.* 182 (1989) 319–326.
- [73] U.S. The Mathworks Inc., Natick, Massachusetts, MATLAB and Statistics Toolbox Release 2012a, (n.d.).